

Project Outside of Course Scope

Head movement in the diffusion and resting-state functional magnetic resonance imaging (MRI) data of the Adolescent Brain Cognitive Development (ABCD) study

Author: H. A. Georgiev (wfg874)

Advisor: Melanie Ganz-Benjaminsen

Date: January 31, 2024

Contents

1	Introduction	3
2	Background	3
2.1	Principles of MRI	3
2.2	Properties of k-space	4
2.3	Motion	6
2.4	Decomposing a 3×3 rotation matrix	6
2.5	Registration	7
2.6	The ABCD study	7
3	Methods	8
3.1	Population	8
3.2	Brain imaging protocol	8
3.3	Motion metrics	9
3.4	Motion study	9
3.4.1	Spatial analysis	9
3.4.2	Temporal analysis	9
3.4.3	Correlation analysis	9
3.4.4	Statistical testing	9
4	Results	10
5	Discussion	19
5.1	Understanding motion	19
5.2	Spatial analysis	19
5.3	Temporal analysis	20
5.4	Correlation analysis	20
5.5	Limitations and future work	21
5.6	Code availability	21
6	Conclusion	21

Abstract

Magnetic Resonance Imaging (MRI) is our most potent tool for brain imaging due to its harmlessness and soft-tissue contrast. Nonetheless, MRI is susceptible to artifacts, often caused by the head motion of the subject within the scanner. This problem is particularly prevalent in children, who are often intimidated by the procedure. Previous studies have investigated the issue and attempted to limit the effects of head motion through various techniques, such as anesthetizing the children [1], distracting them with visual and sonic stimuli during the acquisition time, or simply preparing them before the procedure starts. Although achieving some noticeable results, the previously mentioned strategies face several limitations, including potential health complications for the subjects and an extended preparation period. Therefore, patients and medical staff would greatly benefit from further optimization of the current methodology.

The success of optimization hinges on careful analysis of the motion tendencies of children. A deeper insight into how they move during scanning would substantially improve retrospective motion correction. A potential breakthrough in the field would come with reduced health complications for the subjects and alleviation of scanning costs. The project aims to understand children's motion by investigating the Adolescent Brain Cognitive Development (ABCD) study. Functional and diffusion-weighted MRI (fMRI/dw-MRI) are the study's concerns, as motion could render them futile for diagnosis. Consequentially, the motion correction matrices for the fMRI and dw-MRI time series will be examined to evaluate the presence or absence of statistically significant differences between subjects of different sexes and ages.

1 Introduction

The major limitation of Magnetic Resonance Imaging (MRI) is its susceptibility to motion artifacts caused by the subject's head movement inside the scanner. However, this makes the modality somewhat dependent on subject cooperation, an amplified issue when working with children more intimidated by the procedure than adults. Motion leads to undersampling of the k-space, which usually manifests as ghosting or blurring [2] and hinders the future diagnosis of the scan.

Several approaches are used to mitigate the effect of motion artifacts on the acquired scan with different amounts of success, including preparing the child by introducing it to a mock scanner [3], anesthetizing it [1], updating the scanner's field of view in real-time (prospective analysis), or registering a sequence of scans to one of them [4] (retrospective analysis).

Unfortunately, the first two methods come at a substantially increased cost and longer queues [1], as they would require the presence of multiple experts. Furthermore, some children require scans annually, and exposing them to general anesthesia that frequently could potentially affect their cognitive development [5]. On the other hand, prospective and retrospective analysis depend on profound understanding of children's motion patterns to achieve optimal results.

This paper studies the motion curves of a large cohort of children. The subjects will be divided into separate groups based on age and sex, thus achieving the study's primary goal - concluding whether significant differences in motion traits of the sub-populations exist. The research is complemented by temporal and correlation analysis, which studies the motion change over time and any possible correlations between different movements.

2 Background

2.1 Principles of MRI

The harmlessness of an MRI scan is due to the nature of the procedure. Unlike X-rays and tomography, MRI does not rely on ionizing radiation but the nuclear magnetic resonance phenomenon. The MRI takes advantage of the abundant hydrogen protons inside the human body. Those protons behave like a dipole, spinning around their axis and creating a tiny magnetic charge. Once a strong magnetic field is applied, as is the case inside a scanner, the protons will align with the field. Consequentially, all protons will have the same frequency and average phase. However, it is impossible to distinguish tissues based on their MR signal once all protons align with the magnetic field. Therefore, a radio frequency (RF) pulse that forces the proton into either a 90° or 180° realignment with the field is applied [6] [7]. Stopping the RF pulse would allow the proton to realign with the field

again, releasing an MR signal, which is captured and saved onto the k-space [6]. This procedure is carried out for all positions to achieve unambiguous encoding of the MR signal, and it is captured mathematically by the Larmor equation:

$$frequence(p) = \gamma + (B_0 + G * p) \quad (1)$$

where p is the position, γ is the gyromagnetic ratio (unique for atomic species), B_0 is the scanner's magnetic field, and G is the radio frequency applied along the position axis[6].

2.2 Properties of k-space

As mentioned in subsection §2.1, the MR signals are stored in the k-space (see Figure 1a)- for simplicity, the paper assumes a 2D k-space; however, the properties easily extend to higher dimensions. The precise (k_x, k_y) k-space location of the data from a sampling point is given by the following pair of equations:

$$k_x(t') = \int_0^{t'} \gamma G_x(t) dt \quad k_y(t') = \int_0^{t'} \gamma G_y(t) dt \quad (2)$$

where γ is the gyromagnetic ratio, $G_{x/y}(t)$ is gradient strength at some time point t , t' is the time point at which a data sample is acquired, and the k-space coordinates represent spatial frequencies [6]. From the pair of equations in (2) follows the first important property of the k-space:

1. The strength of the gradient determines the data point's position in the k-space with respect to the origin ($k_x = 0, k_y = 0$)[6].

We can crudely generalize MR signals as low and high-spatial-frequency signals. Relatively uniform regions produce the former type, while the latter results from encountering the region's edges, where a sharp change of intensities is observed [7]. An important question is where precisely each region should be stored in the k-space. This leads to the second k-space property:

2. Low-spatial-frequency signals are stored near the origin (center) of the k-space, while high-spatial-frequency signals are stored around the periphery[6].

To appreciate the following two properties of the k-space, one should be familiar with the Fourier Transform (FT). FT is a lossless transformation tool that translates information from one domain to another. In the case of MRI, the inverse of the FT (IFT) is used to reconstruct the spatial coordinates (x, y) of the image from the spatial frequencies (k_x, k_y) of the k-space [6]. Finally, this leads us to properties three and four:

3. Starting at the origin and progressively increasing the amount of spatial frequencies used for reconstruction improves the spatial resolution of the image substantially [7].
4. The low-spatial-frequencies carry more information than the high-spatial-frequencies [7].

Based on the discussed properties of the k-space, we can draw the following conclusions:

- There is no one-to-one correspondence between k-space and image points (and vice versa). Consequentially, every point in the k-space influences every image point, and every image point is influenced by every k-space point [6] [7].
- The influence of a k-space point on the image is determined by the point's location in the k-space [7]. As shown in Figure 1b, points closer to the k-space's edges contribute to the resolution of the image, while points around the k-space center determine the overall image contrast.
- The regions controlling the resolution and overall contrast are not divided by a specific threshold [7]. Changing the cut-off diameter results in a gradual change in image quality (see Figure 1c).

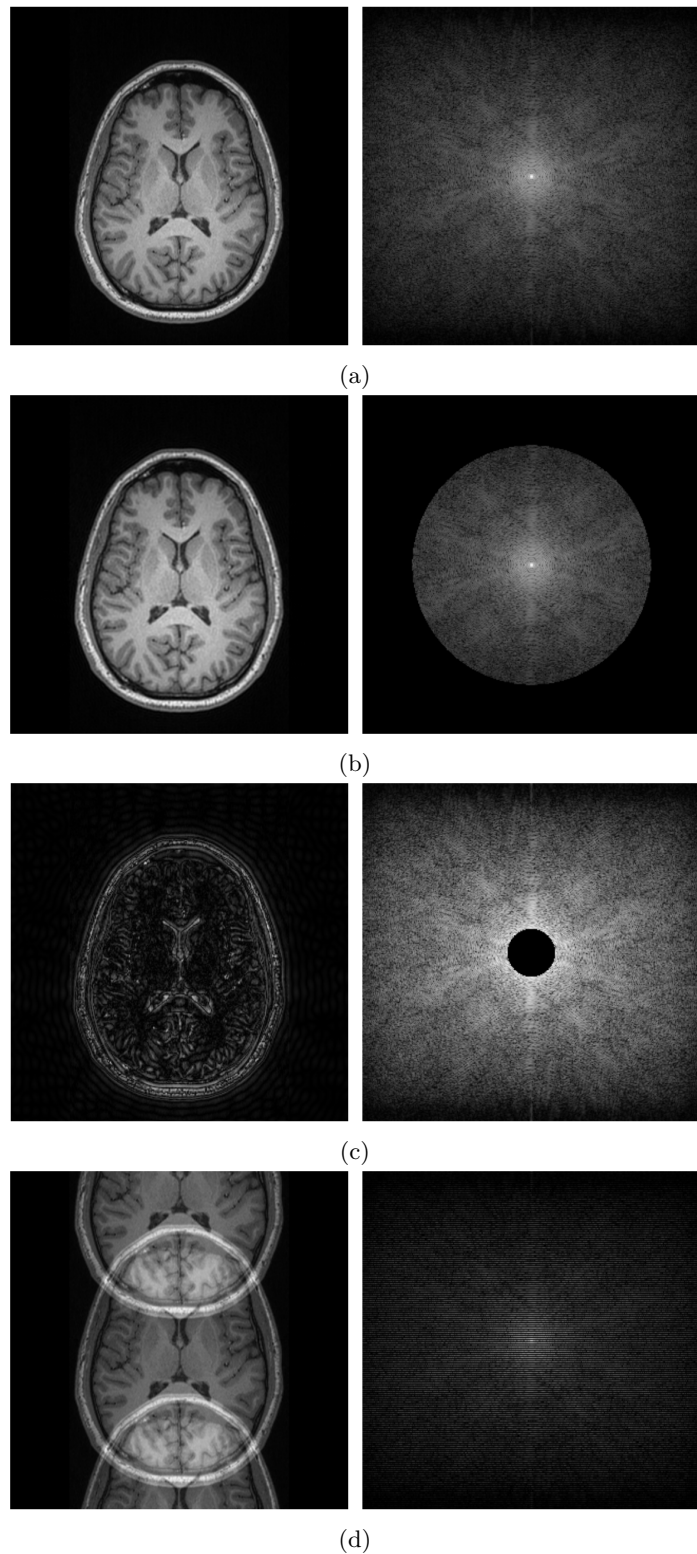


Figure 1: An example of a brain image (left), its k-space (right) (a) and the effects on applying a low-pass filter (b), high-pass filter (c), and undersampling (d) (Examples taken from my hand-in 1 in the Medical Image Analysis course on DIKU).

2.3 Motion

Despite the subject's effort to remain still during acquisition time, involuntary motions are impossible to evade. For example, body fluids will not cease to travel through the body as long as the subject is alive. Similarly, the subject cannot control tissue movement caused by peristalsis and respiration. Such movements fall into the category of flow and elastic body motion. While a flow can be described as a velocity vector of different complexity, elastic body motion can be accounted for by a matrix with 12 degrees of freedom (DOF) [2].

However, the primary concern of this study is head movement and its effects on fMRI and DTI. Unlike elastic body motion, which causes many non-linear local deformations and displacements, head movement fully preserves the subject's shape. Consequentially, it can be represented using 6 DOF: rotation around and translation along the X , Y , and Z -axis [2]. Therefore, all possible head movements inside the scanner fall within a subset of the affine transformations, known as rigid body transformations.

Head rotations during scanning introduce an identical rotation of the spatial frequency components concerning the encoding gradients, which ultimately redistributes the samples in k-space. As a result, the assumption that k-space points are sampled uniformly, hence fulfilling the Nyquist criterion, is violated [2] (see 1d). Since the violation is local, some points will be measured multiple times, while others will be ignored. This phenomenon is known as a spin history effect. Furthermore, by a property of the Fourier Shift theorem, a spatial translation induces a phase modulation in the frequency domain. The outcome of such an event is often a blurrier image [2].

2.4 Decomposing a 3×3 rotation matrix

Quantifying the precise amount of rotation is a necessary step in motion correction. Since human bodies are three-dimensional, a 3×3 matrix is required to capture all possible head movements. The general form of such a matrix is as follows:

$$R = \begin{bmatrix} r_{11} & r_{12} & r_{13} \\ r_{21} & r_{22} & r_{23} \\ r_{31} & r_{32} & r_{33} \end{bmatrix}$$

The rotation matrix R can be decomposed into the product of three separate matrices, each of which describes the rotation around one of the principle axes:

$$R = \underbrace{\begin{bmatrix} 1 & 0 & 0 \\ 0 & \cos\alpha & -\sin\alpha \\ 0 & \sin\alpha & \cos\alpha \end{bmatrix}}_{R_X} \underbrace{\begin{bmatrix} \cos\beta & 0 & \sin\beta \\ 0 & 1 & 0 \\ -\sin\beta & 0 & \cos\beta \end{bmatrix}}_{R_Y} \underbrace{\begin{bmatrix} \cos\gamma & -\sin\gamma & 0 \\ \sin\gamma & \cos\gamma & 0 \\ 0 & 0 & 1 \end{bmatrix}}_{R_Z}$$

where R_X corresponds to rotation around the X -axis, R_Y around the Y -axis, R_Z to rotation around the Z -axis [8], and α , β , and γ are the Euler angles describing the patient's head orientation with respect to the scanner's coordinate system. Unlike factor multiplication, matrix multiplication is not commutative, that is, $R_X R_Y R_Z \neq R_Z R_Y R_X$, and in this particular case.

The exact values of $R_{11} \dots R_{33}$ in this particular case are given by the $R_X R_Y R_Z$ product:

$$\underbrace{\begin{bmatrix} \cos(\beta)\cos(\gamma) & -\cos(\beta)\sin(\gamma) & \sin(\beta) \\ \sin(\alpha)\sin(\beta)\cos(\gamma) + \cos(\alpha)\sin(\gamma) & \cos(\alpha)\cos(\gamma) - \sin(\alpha)\sin(\beta)\sin(\gamma) & \sin(\alpha)(-\cos(\beta)) \\ \sin(\alpha)\sin(\gamma) - \sin(\alpha)\cos(\beta)\sin(\gamma) & \sin(\alpha)\cos(\gamma) + \cos(\alpha)\sin(\beta)\sin(\gamma) & \cos(\alpha)\cos(\beta) \end{bmatrix}}_R$$

Based on the entries of the rotation matrix R , the Euler angles can be obtained using the following set of equations:

$$\alpha = -\arctan\left(\frac{R_{23}}{R_{33}}\right) \quad \beta = \arcsin(R_{13}) \quad \gamma = -\arctan\left(\frac{R_{12}}{R_{11}}\right) \quad (3)$$

For the sake of completeness, there is an inherent flaw with Euler angles related to the possible loss of DOF, which is avoided by dividing by ϵ if R_{33} or R_{11} equal zero. This problem is referred to as a Gimbal lock [9]. However, this is not a concern in head motion, as the human neck naturally does not allow for movements that would lead to it, consequentially preserving all DOF.

2.5 Registration

Motion correction involves the registration of all scans in the fMRI time series to a single scan of the time series. The registration process aims to find a transformation T that maximizes some measure of similarity between the floating image X (the one being transformed) and the reference image Y (the one which we transform to). A common choice for Y is the first or middle image of the time series [4]. Mathematically, registration can be defined as:

$$T^* = \arg \min_{T \in S_T} M(Y, T(X)) \quad (4)$$

where T^* is the transformation of X that maximizes the similarity measure M between X and Y . The search for T^* is carried over the set of all allowable transformation S_T , which in the case of motion correction is the set of all rigid transformations [4].

The search of T^* will result in a transformation matrix that has the following definition:

$$T = \begin{bmatrix} R_i & \vec{d}_i \\ 0 & 1 \end{bmatrix}$$

where R_i is a 3×3 matrix specifying the rotation and \vec{d}_i is a 3×1 vector specifying the displacement of the i^{th} image [8]. Note that here i refers to the floating image X .

Since motion correction is performed in a three-dimensional space, the rotation matrix R_i can be decomposed into three separate matrices, each of which defines how the object rotates in space along the X -, Y -, and Z -axis:

$$R_i = \underbrace{\begin{bmatrix} 1 & 0 & 0 \\ 0 & \cos\alpha_i & -\sin\alpha_i \\ 0 & \sin\alpha_i & \cos\alpha_i \end{bmatrix}}_{R_{i\alpha}} \underbrace{\begin{bmatrix} \cos\beta_i & 0 & \sin\beta_i \\ 0 & 1 & 0 \\ -\sin\beta_i & 0 & \cos\beta_i \end{bmatrix}}_{R_{i\beta}} \underbrace{\begin{bmatrix} \cos\gamma_i & -\sin\gamma_i & 0 \\ \sin\gamma_i & \cos\gamma_i & 0 \\ 0 & 0 & 1 \end{bmatrix}}_{R_{i\gamma}}$$

Similarly, each of \vec{d}_i 's entries denote the displacement along the corresponding axis:

$$\vec{d}_i = [d_x \ d_y \ d_z]^T$$

Consequently, we allow for six degrees of freedom (DOF): a rotation around and a displacement along each axis [4] [8].

One of the benefits of matrices and vectors is that we can combine them into a single matrix that describes some space transformation. If one were to stack R_i and \vec{d}_i , the result would be a 3×4 matrix. Such an approach is far from ideal, as non-square matrices have no inverse, which violates the fact that all motions in the scan can be undone. For example, if the subject moves their head along the X -axis by a certain amount, they can move it back by the same amount in the opposite direction, hence reaching their starting position. For this reason, an extra row is added at the bottom of the matrix, which contains zeros at all entries, except for the right-most one, which plays the role of a scale factor. As we allow only for rigid transformations, the value of this entry is set to 1.

2.6 The ABCD study

The Adolescent Brain Cognitive Development (ABCD) study¹ is a large, long-term study of biological and behavioral development in the United States. Between 2016 and 2018, 11,875 children of various ethnic and educational backgrounds joined the program and participated in baseline scans. All children were 9-10 years old, and the final scans will take place in 2027, giving the consortium data about the individuals' brain development spanning a decade.

The study assesses many brain functions, such as physical and mental health, neurocognition, and social and emotional development, by collecting biosamples from the children, organizing various tests, and scanning their brains. The brain scans are what this paper will focus on in its analysis. The ABCD consortium comprises a Coordinating Center, Data Analysis, Informatics & Resources Center, and 21 research sites where data is collected².

¹See: <https://abcdstudy.org/about/>

²See: <https://abcdstudy.org/scientists/>

3 Methods

3.1 Population

This paper investigates how children move at scan time and whether there are statistically significant differences between movement traits of different sub-populations. Subjects are divided into four groups based on sex and age: 9-year-old males and females and 10-year-old males and females. Table 1 presents a summary of the groups. Note that the ABCD study reports subjects' ages in months on the registration day. However, scans are not immediately taken, and this paper considers only those who were 9 and 10 at the time of the scan.

Table 1: Summary of each sub-population's number of participants per modality.

Number of participants per modality	9-y-o. males	9-y-o. females	10-y-o. males	10-y-o. females
rsfMRI	2,509	2,358	2,415	2,116
DTI	595	536	531	484

It is important to note that children of inter-gender identity and those who failed to provide their exact age (in months) have yet to be included in the analysis due to their diminutive number. Such a decision is based on the difficulty of arguing statistical significance for small populations.

3.2 Brain imaging protocol

As the ABCD study is conducted in 21 sites, a well-defined imaging protocol³ is essential to ensure consistency and replicability across sites and scanner vendors. Therefore, every participating child undergoes a standardized sequence of steps, maintaining consistency before, during, and after the scanning process.

Of particular interest for this paper are the rsfMRI and DTI scans. The former is conducted in two 10-minute blocks, each split into multiple 2-5-minute runs. Furthermore, children are not obligated to participate in a given number of runs and can decide to stop after any of them. Consequentially, there is no fixed number of runs between subjects: one might go through four 5-minute runs, while another might decide to stop after the first run, which only took 2 minutes. In stark contrast, the DTI scan occupies the time frame between the two rsfMRI sessions, encompassing a continuous 9-10-minute scan. Another critical distinction between rsfMRI and DTI is that children are shown a movie during the latter (see Table 2 for a summary of the protocol).

These dissimilarities in the two modalities are noteworthy as they influence how children behave inside the scanner. The experiments in §3.4 provide a more detailed exploration of these intricacies.

Table 2: An abridged version of the ABCD baseline protocol brochure's page 9. Legend:  - children were not distracted during the scan,  - children were shown a movie during the scan.

Scan module	Protocol	Runs	Duration (min)	External stimuli
Scan (inside scanner)	Set-up	-	3-6	-
	rsfMRI	2-5	10 (max)	
	DTI	1	9-10	
	rsfMRI	2-5	10 (max)	
	N-Back Task	1	12	

³See page 9 of https://abcdstudy.org/wp-content/uploads/2019/12/Brochure_Protocol-Baseline-eg.pdf.

3.3 Motion metrics

The frame-wise displacement quantifies the instantaneous head motion of the subject inside the scanner [8]. Such quantity can be obtained by taking the sum of the absolute displacement along each DOF:

$$FD_i = |\Delta d_{ix}| + |\Delta d_{iy}| + |\Delta d_{iz}| + |\Delta \alpha_i| + |\Delta \beta_i| + |\Delta \gamma_i| \quad (5)$$

where $\Delta d_{ix} = d_{(i-1)x} - d_{ix}$ is the absolute displacement along the x -axis between the i^{th} and $(i-1)^{th}$ subjects [8]. The other displacement coefficients are obtained in a similar fashion.

For the above calculation to hold, using the same units for translation and rotation is crucial. Therefore, radians are converted to millimeters by calculating the surface displacement of a sphere with a radius of 50 mm [8]. The value is not chosen arbitrarily - it is approximately the mean distance between the cerebral cortex and the center of mass:

$$d = r\Delta\sigma$$

where r is the radius, and $\Delta\sigma$ is the central angle in radians, corresponding to α , β and γ .

3.4 Motion study

This study aims to investigate the nature of motion comprehensively by looking at it from three unique perspectives: spatial (§3.4.1), which analyzes how children move in all three dimensions; temporal (§3.4.2), which answers the question of how children move at different stages of the procedure; and lastly, the dependency between different movements (§3.4.3). The applied statistical analysis (§3.4.4) evaluates the dissimilarity between population groups.

3.4.1 Spatial analysis

The primary focus of this study is to explore potential discrepancies in movement traits of the sub-populations. Such analysis is done by comparing different groups' greatest absolute displacement distribution. Motion is described as translation along and rotation around the X , Y , and Z -axis, consistent with the outlined approach in §2.3 and §2.4. The experiment also accounts for outliers by comparing their number per motion for both genders and modalities.

3.4.2 Temporal analysis

An important aspect of motion analysis is understanding how children move throughout the various procedure stages. One way to distill such insight is to compare the greatest absolute displacement in each rsfMRI run. As discussed in §3.2, the number of rsfMRI runs varies between subjects. Examination of the entire population showed that 76.3% of children experienced four runs, with an additional 8.9% experiencing four or more runs — this combined sub-population of 85.2% of the subjects is precisely the focus of this experiment. Only the first four runs of every subject are considered to ensure a fair comparison between the two groups.

3.4.3 Correlation analysis

The final aspect of motion analysis is to quantify the degree of relationship between various motions. For this purpose, the linear correlation between all motion types is measured by the Pearson correlation coefficient (PCC), resulting in a 6×6 correlation map for the entire population. Such a map would give insight into how change in one variable affects another, answering whether there is a correlation between translations along X and rotations along Y in a given population, for example.

The decision to present the results for the entire population and not for groups is based on their similarities. As a result, it was more fitting to avoid distracting the reader with four times as many figures when the conclusions would be the same.

3.4.4 Statistical testing

All statistical testing is performed using the non-parametric Mann-Whitney U-test to account for the possibility that the compared populations might not be normally distributed.

4 Results

Figure 2a and 2b show the motion curves of a randomly selected 9-year-old male subject's rsfMRI scan. Each motion curve represents the displacement along or rotation around an axis at a given frame, where one frame is obtained over 2 seconds. The relationship between the brain and axes is visualized in Figure 2c.

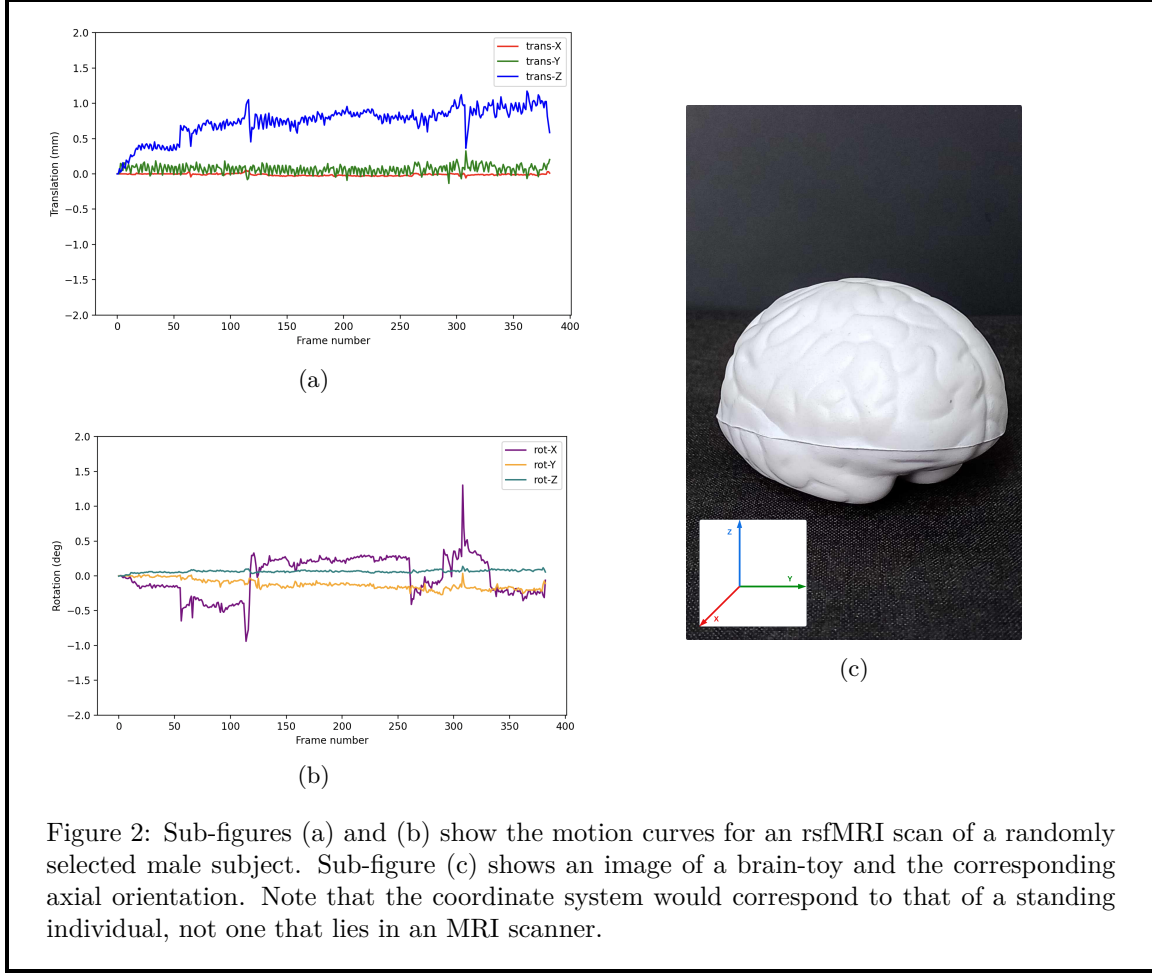


Figure 2: Sub-figures (a) and (b) show the motion curves for an rsfMRI scan of a randomly selected male subject. Sub-figure (c) shows an image of a brain-toy and the corresponding axial orientation. Note that the coordinate system would correspond to that of a standing individual, not one that lies in an MRI scanner.

The box plots compare the mean, median, and greatest absolute translational and rotational displacement for males and females aged 9 (see Figure 4 for rsfMRI and Figure 6 for DTI) and 10 (see Figure 5 for rsfMRI and Figure 7 for DTI). Note that all male distributions' absolute minimum and maximum values and the mean and median are greater for rsfMRI and of similar magnitude to female distributions for DTI. The distributions' standard deviation values in Table 3 also indicate larger spread in male distributions, with the only exception being translation along Y in DTI scans for 10-year-old children.

Older children also showed smaller standard deviations and fewer outliers in rsfMRI (see Table 4 and Table 5) across all axes and sexes than the younger sub-population. A similar pattern is observed in DTI scans (Table 6 and Table 7), except for females' translation along Y. Furthermore, male subjects tend to produce more outliers for translation motion. In comparison, female ones tend to produce more outliers for rotation motion. Such observation holds to a certain degree for both modalities.

A noteworthy detail is the substantial decrease in motion during DTI scans, especially in translation along Y and Z and in rotation around X: the motion components that dominated rsfMRI scans. When comparing the box plots of the two modalities, a 5 to 8-fold decline is observed for the greatest absolute displacement. This observation, combined with fewer scans and outliers for DTI,

Table 3: Summary of sub-populations’ standard deviation across different modalities and motions. All values are rounded to the third decimal digit.

Motion	rsfMRI				DTI			
	9-yo m	9-yo f	10-yo m	10-yo f	9-yo m	9-yo f	10-yo m	10-yo f
trans-X	3.173	2.806	2.784	2.358	0.606	0.517	0.526	0.478
trans-Y	7.414	6.891	6.026	4.439	1.117	0.992	0.993	1.037
trans-Z	8.674	7.888	7.357	6.401	1.296	1.138	1.172	1.085
rot-X	10.691	9.342	8.978	7.515	1.224	1.158	1.129	1.094
rot-Y	3.972	3.41	3.532	2.9	0.795	0.733	0.708	0.667
rot-Z	5.656	4.796	4.673	3.944	0.662	0.532	0.53	0.487

results in a smaller standard deviation than the corresponding rsfMRI sub-populations across the board.

Despite some rsfMRI distributions’ overlapping mean and median, which often indicate normality, a Kolmogorov-Smirnov test proved none of them as normal. Figure 3 shows a visual demonstration of this phenomenon.

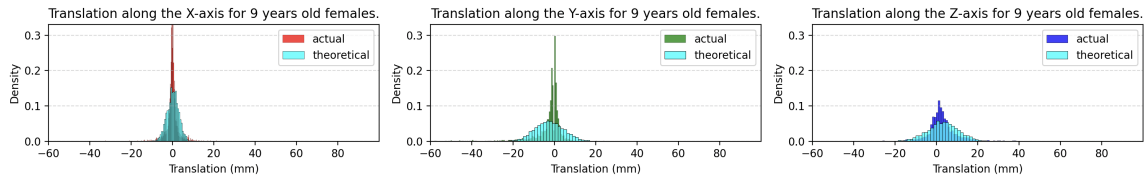


Figure 3: The actual translation distributions for 9-year-old females (red, green, blue) compared to a theoretical normal distribution generated with the actual data’s mean and standard deviation (cyan).

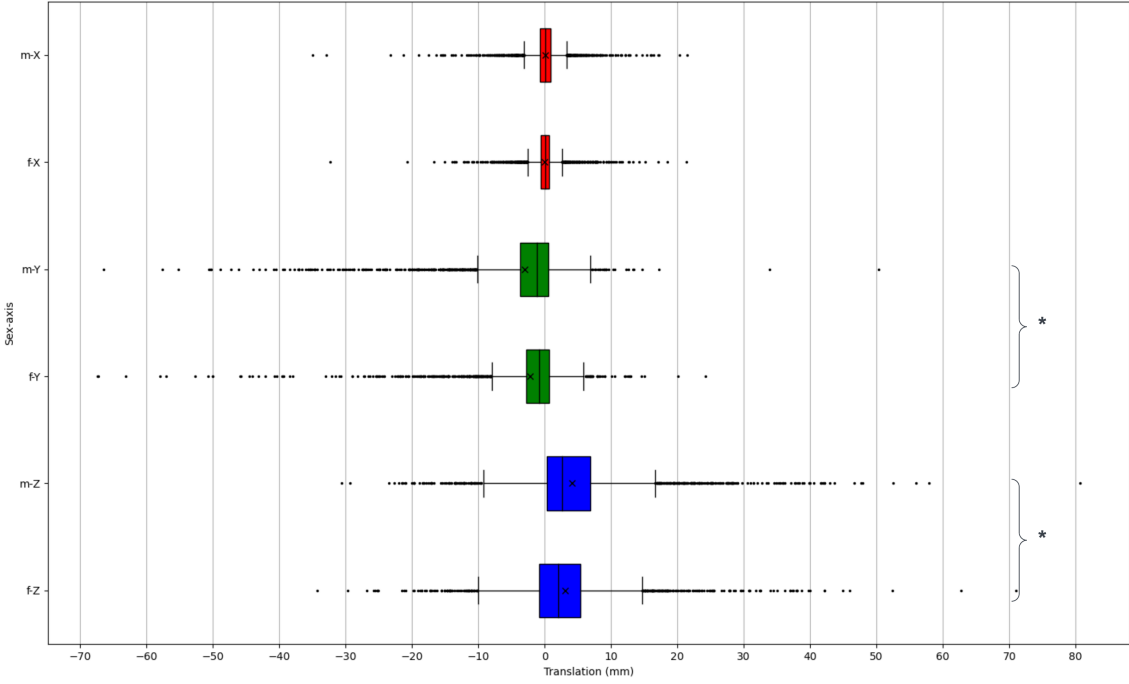
The plots compare the actual translation data with a theoretical normal distribution generated using the actual data’s mean and standard deviation. As one can see, the experimental distribution is skewed excessively compared to the theoretical one.

The pie charts presented in Figure 8 and Figure 9 show the proportion of runs in which the greatest absolute translational and rotational displacement occurred for children aged 9 and 10, respectively. The analysis considers the first four runs of those children who underwent at least four or more. Note that each subject’s run varies in time. Therefore, runs three and four might occur during the first rsfMRI session, the second one, or in different sessions altogether. Finally, the analysis is relevant only for rsfMRI for the reasons discussed in §3.2.

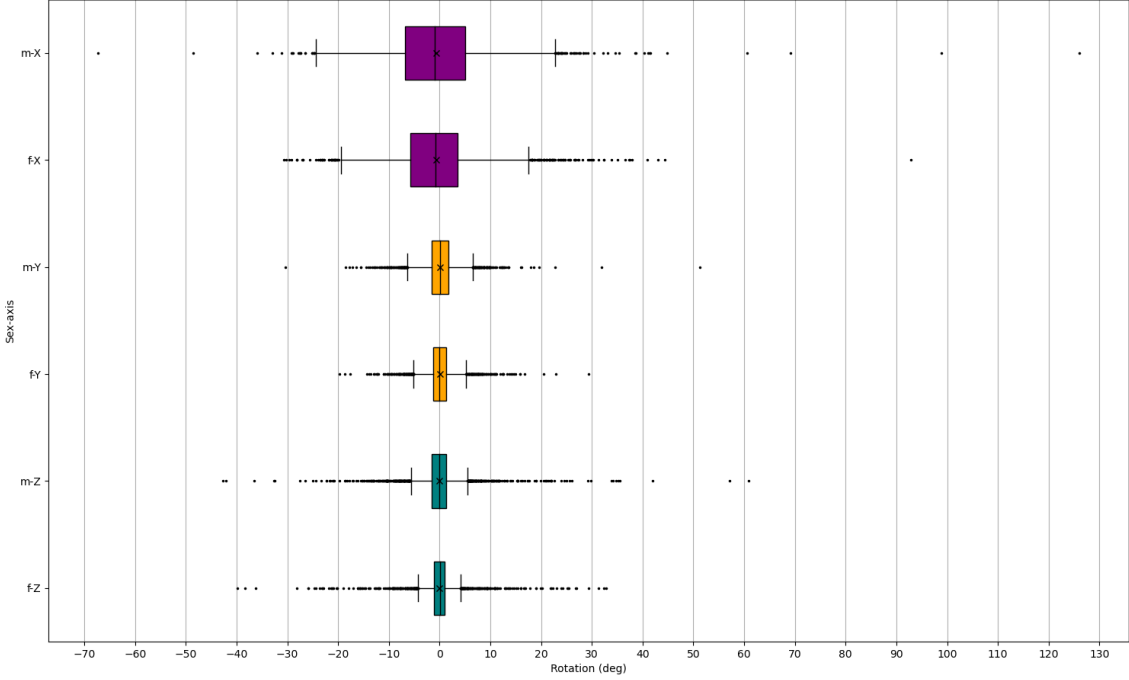
The Pearson correlation coefficient was used to measure the relationship between different movements within each sub-population, and the statistically significant results ($p \leq 0.05$) are reported in Figure 10. The motion pairs that demonstrated the highest positive (*trans-Y* and *rot-X*) and negative (*trans-Y* and *trans-Z*) linear correlation across all sub-populations are compared using 2D histograms (see Figures 11a and 11b). Both distributions have a peak close to the origin and appear somewhat symmetrical.

Note

More data visualization in the form of histograms, similar to those in Figure 3 and Q-Q plots, can be found in the Appendix.



(a)

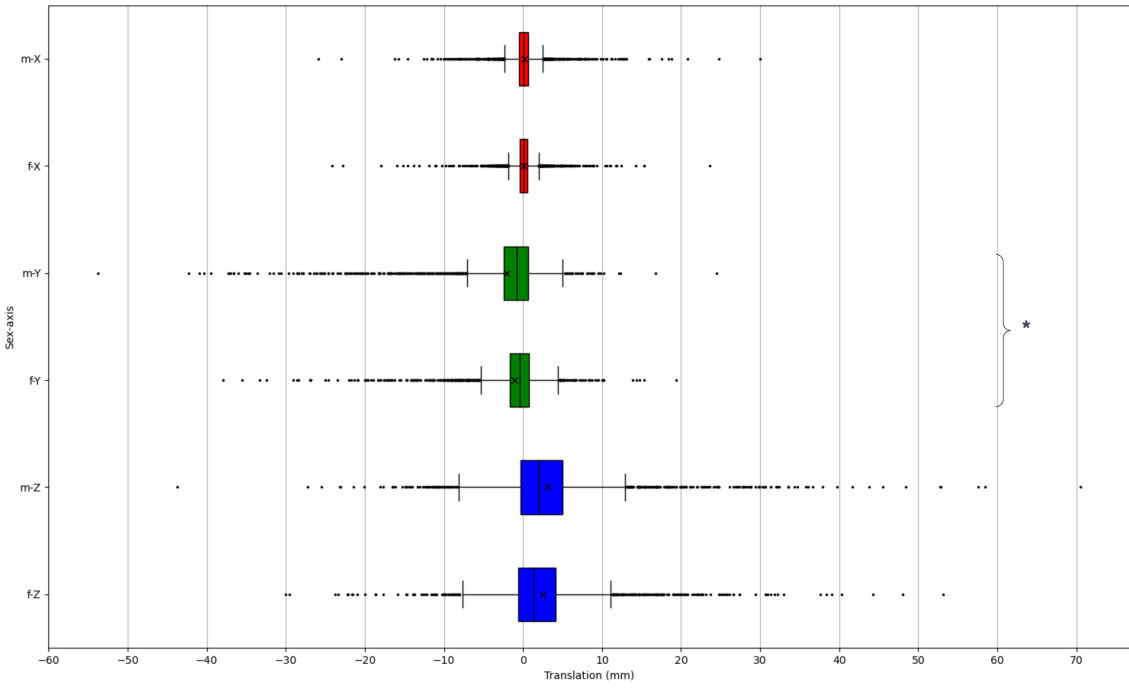


(b)

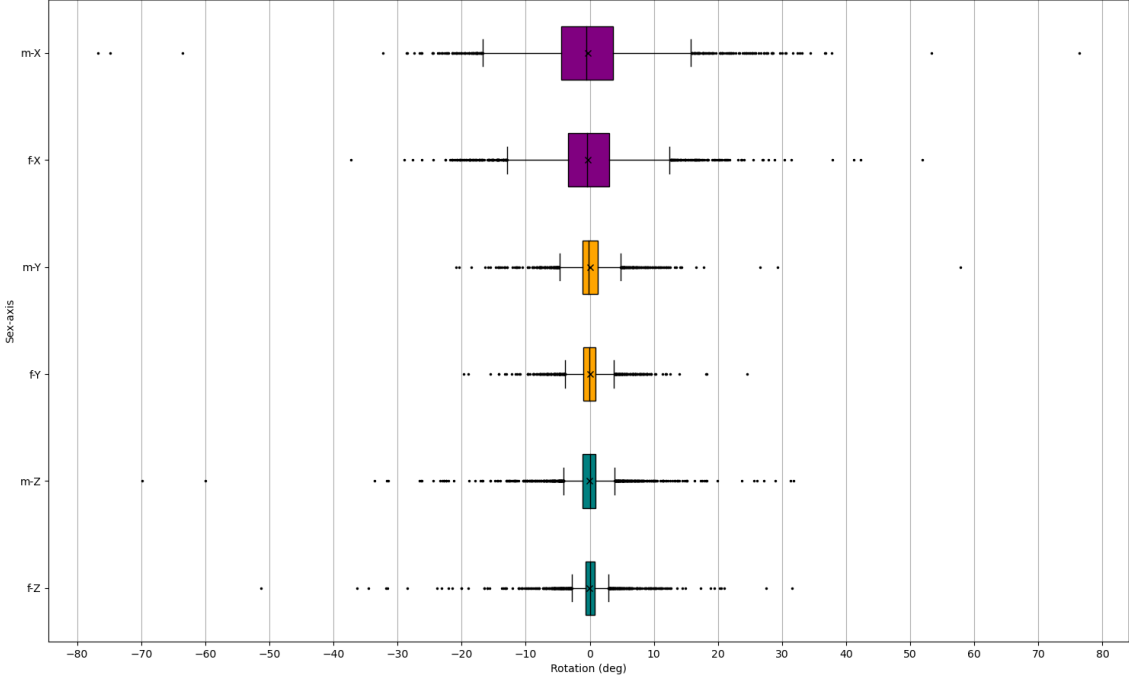
Figure 4: Comparative analysis of translation (a) and rotation (b) displacement in rsfMRI between males and females at the age of 9 years for. Significantly different distributions ($p \leq 0.05$) are denoted with an asterisk (*).

Sex (m/f)	trans-X	trans-Y	trans-Z	rot-X	rot-Y	rot-Z
males	402	286	260	71	233	390
females	399	280	224	128	261	372

Table 4: Outlier counts for each axis in 9-year-old males and females, as illustrated in Figure 2(a) and (b).



(a)

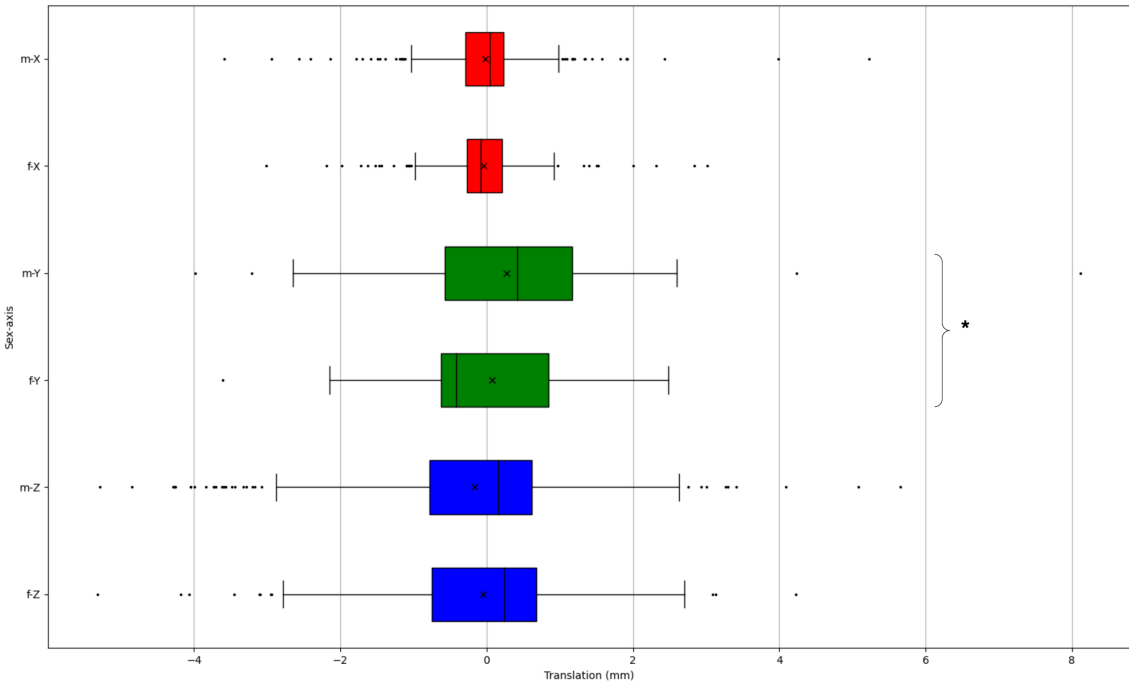


(b)

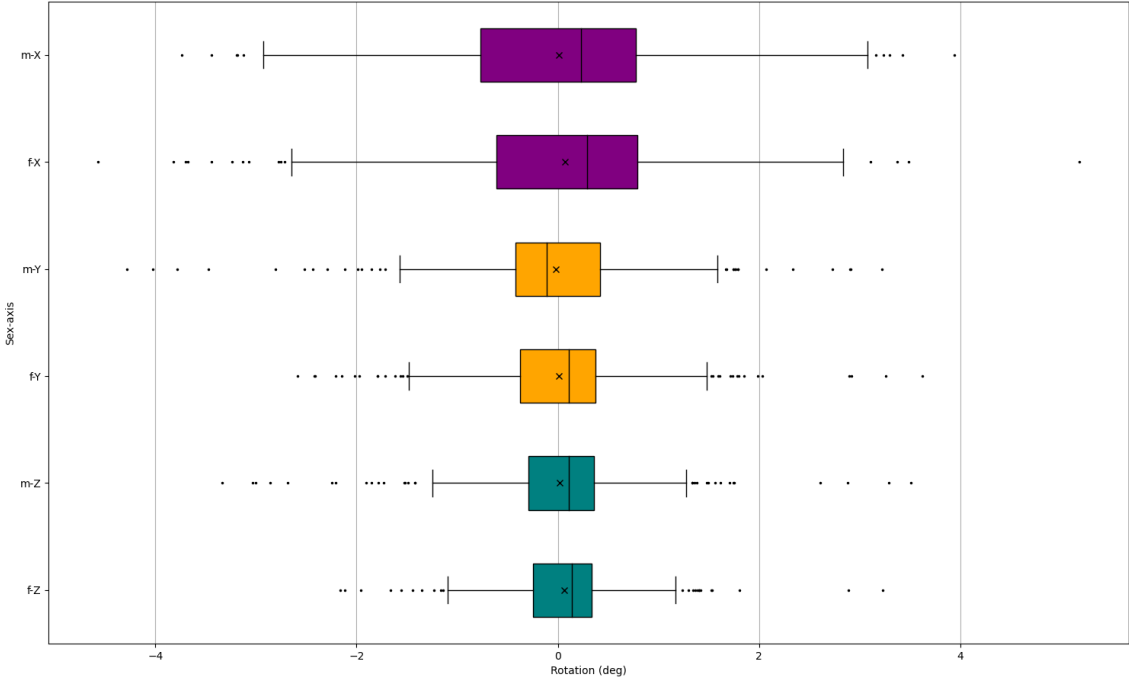
Figure 5: Comparative analysis of translation (a) and rotation (b) displacement in rsfMRI between males and females at the age of 10 years. Significantly different distributions ($p \leq 0.05$) are denoted with an asterisk (*).

Sex (m/f)	trans-X	trans-Y	trans-Z	rot-X	rot-Y	rot-Z
males	396	286	227	169	257	398
females	383	267	206	207	269	388

Table 5: Outlier counts for each axis in 10-year-old males and females, as illustrated in Figure 2(a) and (b).



(a)

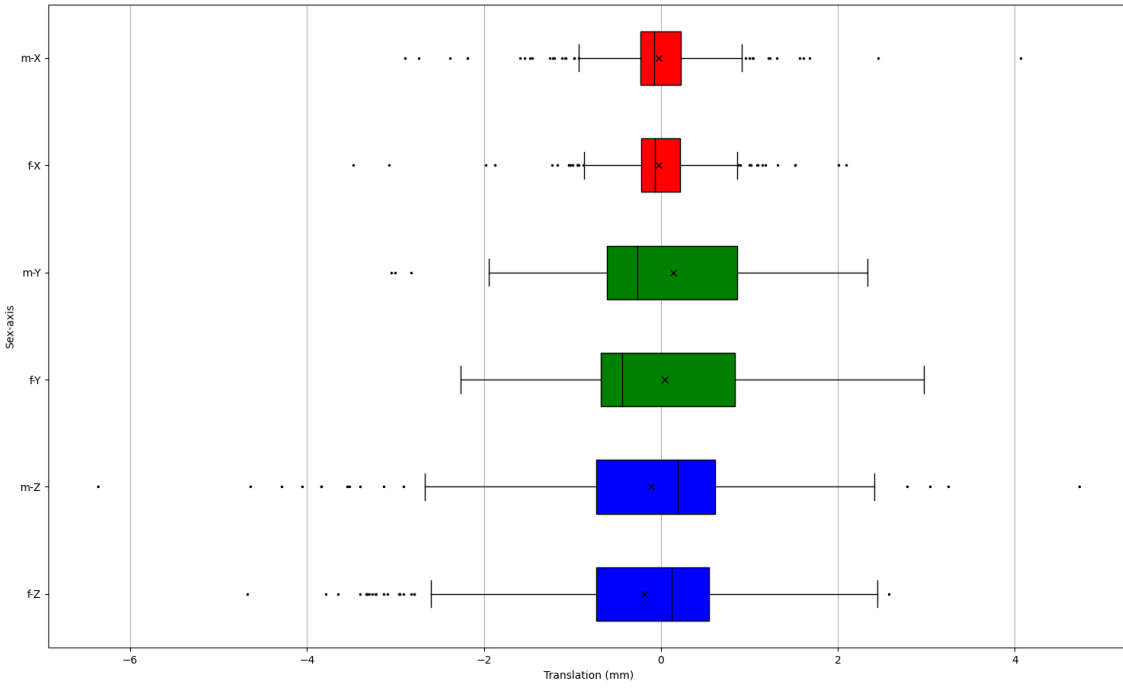


(b)

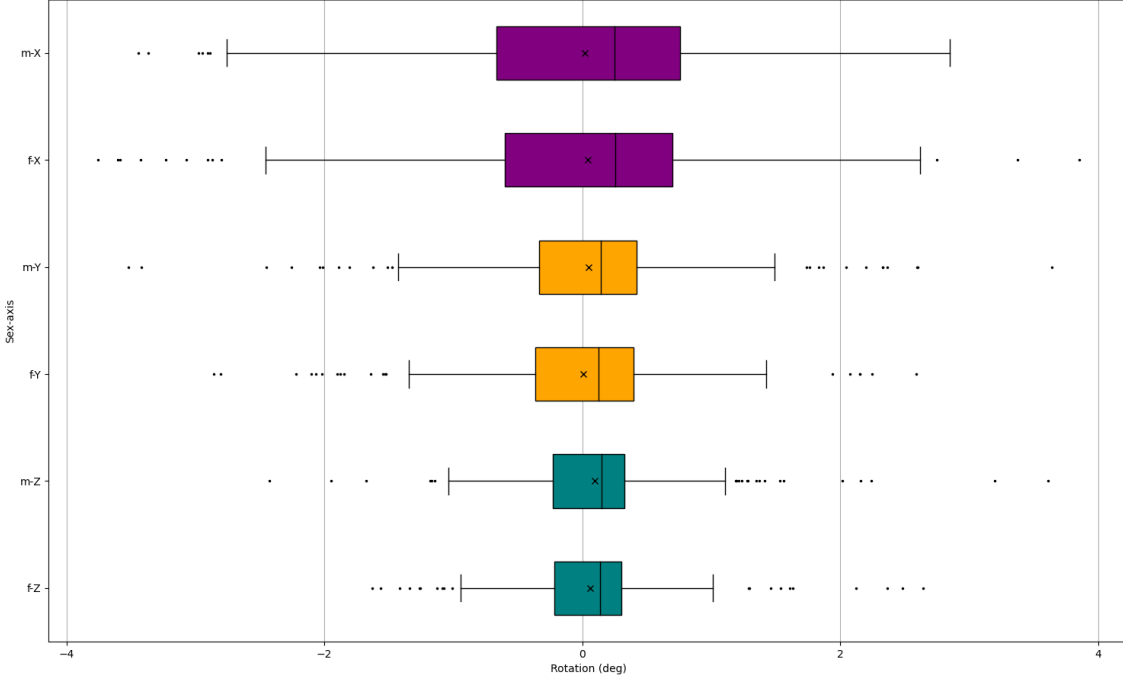
Figure 6: Comparative analysis of translation (a) and rotation (b) displacement in DTI between males and females at the age of 10 years. Significantly different distributions ($p \leq 0.05$) are denoted with an asterisk (*).

Sex (m/f)	trans-X	trans-Y	trans-Z	rot-X	rot-Y	rot-Z
males	33	4	37	31	28	10
females	11	1	24	23	29	15

Table 6: Outlier counts for each axis in 10-year-old males and females, as illustrated in Figure 2(a) and (b).



(a)

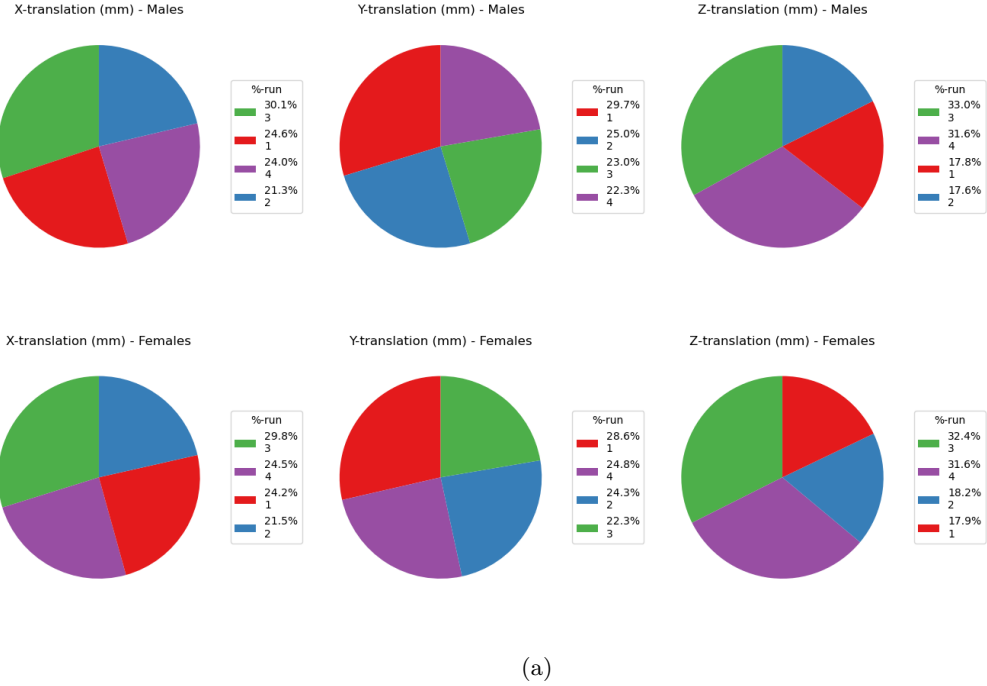


(b)

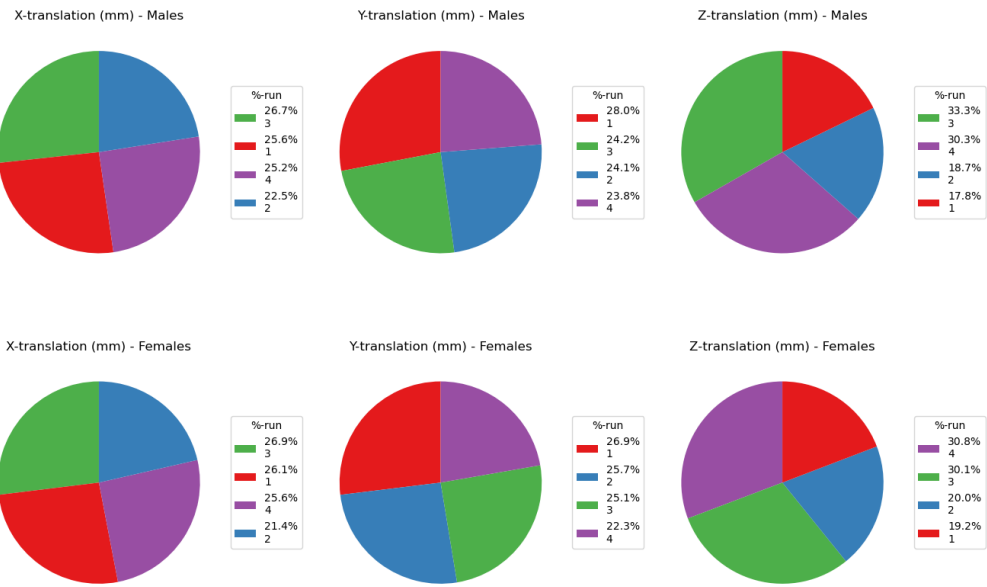
Figure 7: Comparative analysis of translation (a) and rotation (b) displacement in DTI between males and females at the age of 10 years. Significantly different distributions ($p \leq 0.05$) are denoted with an asterisk (*).

Sex (m/f)	trans-X	trans-Y	trans-Z	rot-X	rot-Y	rot-Z
males	15	3	30	22	23	6
females	21	0	27	20	10	12

Table 7: Outlier counts for each axis in 10-year-old males and females, as illustrated in Figure 2(a) and (b).

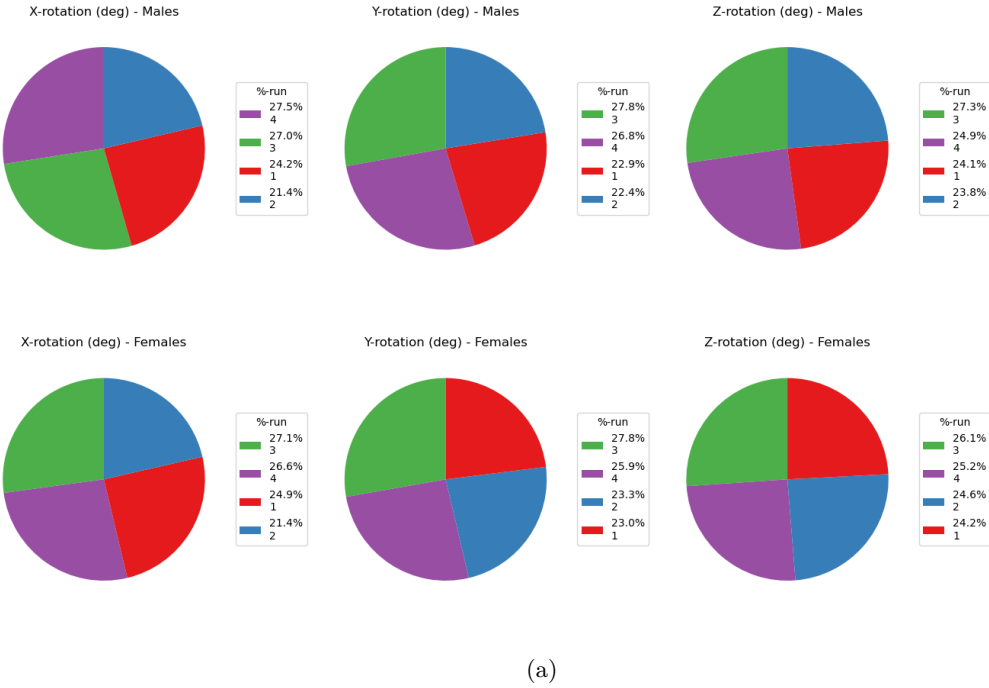


(a)

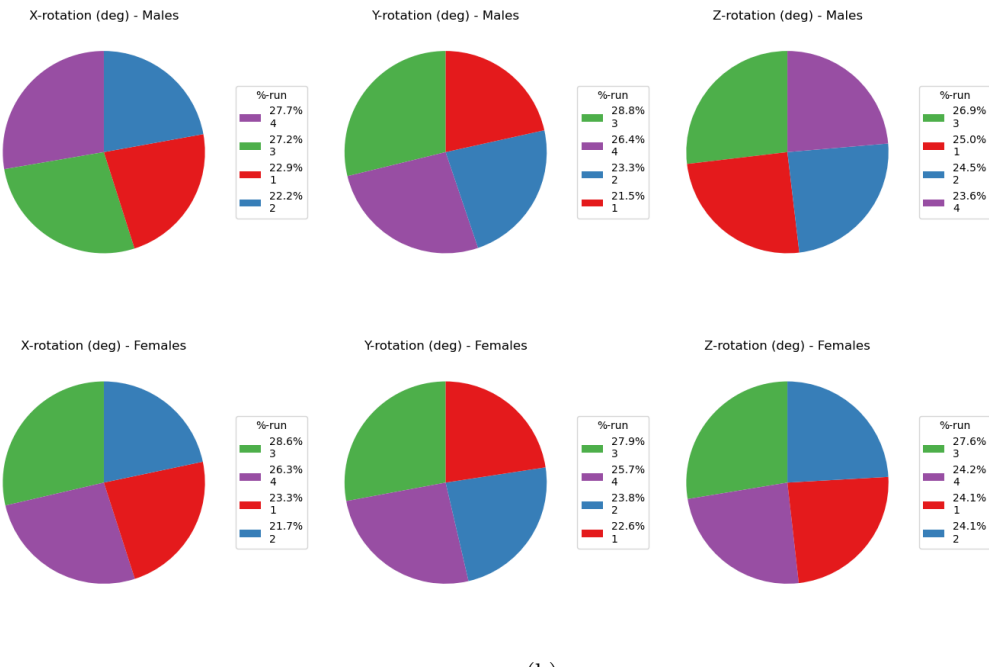


(b)

Figure 8: Proportion of runs in which the greatest absolute translation occurred for 9-year-old (a) and 10-year-old (b) males and females. The plots specifically pertain to the first four rsfMRI runs of subjects who underwent at least four runs. Only subjects with a minimum of four runs are included in the analysis.



(a)



(b)

Figure 9: Proportion of runs in which the greatest absolute translation occurred for 9-year-old (a) and 10-year-old (b) males and females. The plots specifically pertain to the first four rsfMRI runs of subjects who underwent at least four runs. Only subjects with a minimum of four runs are included in the analysis.

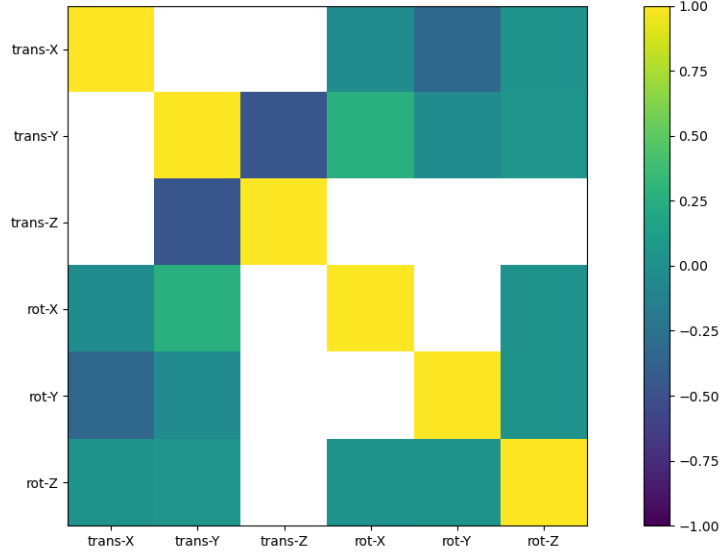


Figure 10: The Pearson correlation coefficient for statistically significant pairs of DOFs (statistically insignificant ones are left blank). The heatmap considers the entire population of rsfMRI scans (no sex-age split).

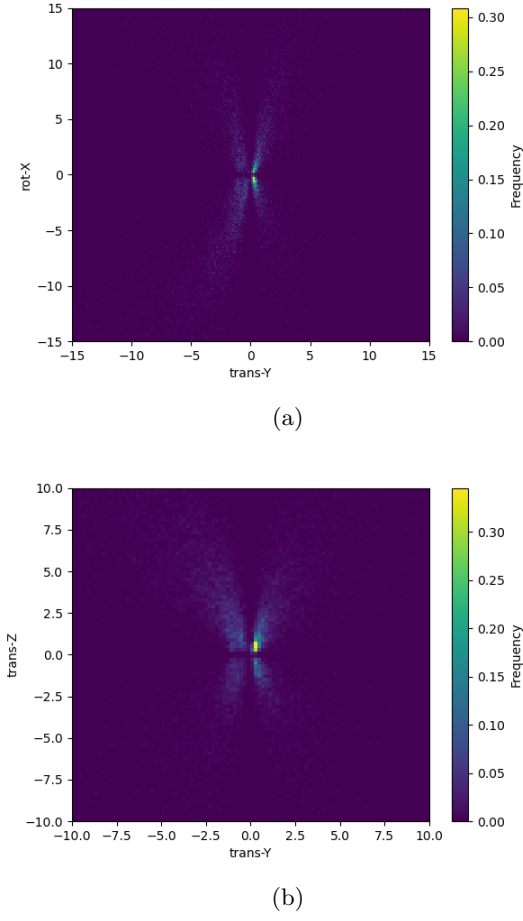


Figure 11: A 2D histogram comparing translation along Y and rotation around X (a) and translation along Y and translation along Z .

5 Discussion

5.1 Understanding motion

A thorough comparison of statistical metrics such as mean, median, greatest absolute displacement (see Figure 4 through 7), and standard deviation (see Table 3) show translation along Y and Z and rotation around X as the dominating source of motion, which resonates with previous finding [1]. All motions above are closely related to innately occurring movements in non-anesthetized subjects [1]. For example, translation along Y and Z corresponds to the child's head sinking in the pillow and body drifting out of the scanner, respectively, while swallowing saliva is often the cause of rotation around X (nodding).

In stark contrast, shaking (rotation around Z), another quiet natural motion, is observed to a far lesser degree. This phenomenon can be explained by the relatively tight head enclosure of the scanner, which limits the subject's movement in that DOF. Similarly, the scanner's dimensions diminish the possibility of excessive translation along X . Finally, rotation around Y , corresponding to somewhat unnatural movement, is seldom observed.

5.2 Spatial analysis

This paper's primary objective is to understand the difference in motion traits between various sex and age groups, given that such a difference exists. The statistical analysis proved only translation along Y as significantly different ($p \leq 0.05$) across 9-year-old males' and females' rsfMRI and DTI scans and translation along Z for rsfMRI scans of children aged 9. Therefore, the discussion will shift focus mainly on these six distributions (marked with "*" in Figure 4 through 7) with occasional remarks on the rest.

An important conclusion that can be made based on the results in Figure 4 through 7 and Table 3 is that males move more across the board, especially for scans that do not involve visual stimuli such as rsfMRI, with translation along Y for females in DTI scans being the exception that proves the rule. Moreover, older children remained stiller during scan time and showed fewer outliers than younger sub-populations (see 4 through 7). These findings are consistent with previously conducted studies [10] [11]. Age proved to be of minor importance when comparing the two sexes, as males aged 10 also moved more than females.

While the reduced amount of motion in scans of different age groups of the same sex can be explained with a certain degree of confidence by the increasing self-control that comes with age, the contrasting movement tendencies between males and females of the same age can be down to two things.

The first and perhaps more attractive of the two potential explanations is sexual dimorphism, which suggests that individuals with larger heads would have less space inside the head coil and move less than those with smaller heads. Previous research has shown that male children have larger brain volumes [12], closely related to the head's size and weight. Consequentially, one might expect that they will move less at scan time. However, the exact opposite is true. Nonetheless, the size difference between the sexes should not be overlooked lightly, as it can explain one of the motion components, namely the translation along Y - heavier heads will sink deeper into the pillow.

A more plausible theory relates to the temperament traits of the sexes. It is well-established that males display higher levels of impulsivity than females [13] [14]. This phenomenon is likely to influence their behavior inside the scanner. It offers a reasonable explanation of males' larger spread (see Table 3) and greater amount of outliers (see Table 4 through 7). In summary, females are the more cooperative group between the two regardless of age or scan type.

Another intriguing observation concerns the presence of external stimuli at scan time. As shown in Table 2, a significant distinction between rsfMRI and DTI is that children were shown a movie during the latter. The result is a substantial decrease of the greatest absolute displacement in the dominant DOFs, with the most noticeable being in rotation around X (approximately 8-fold), while translation along Y and Z experiences a decline of roughly 4-fold (comparison of rsfMRI and DTI results of a given age-sex group). Furthermore, the number of outliers drops from more than 150 for rsfMRI to less than 40 in DTI (see Table 4 through 7). The reduced absolute displacement and

outliers directly influence the spread of the populations, which is much smaller for DTI distributions, as seen in Table 2.

Most importantly, however, incorporating external stimuli, such as playing a movie during image acquisition, is possible for every MRI task that does not strictly require children to keep their eyes closed. Luckily, such MRI tasks are of immense importance in the clinic. Therefore, the future might see general anesthesia for children [1] replaced by visual distraction as a motion reduction measure due to their comparable effect on motion. Such an approach is cheaper and avoids any potential complications caused by anesthesia [5].

5.3 Temporal analysis

The temporal analysis (see Figure 8 and 9) gives another crucial perspective on motion by shedding light on how children move at different rsfMRI stages. Such analysis is necessary to understand whether motion is purely the result of impulsive actions or whether some underlying patterns can be utilized in the clinic.

Starting with the innate movements, males' Figure 8a and females' Figure 8b greatest absolute translation along Y was during the first run for approximately 28.3% of all subjects. An explanation for this observation could be that the head sinks into the soft pillow faster. As the pillow gets denser under the head's weight, it allows for less and less compression. Interestingly, there are many similarities between the sexes' motion patterns for translation along Z (see Figure 8) and rotation around X (see Figure 9) in both age groups. The greatest absolute displacement for both DOFs appears during the latter runs. Furthermore, there is an (almost) perfect overlap in the order of runs and the associated percentage between two age groups of the same sex.

A similar conclusion can be drawn for the other DOFs, namely translation along X (see Figure 8) and rotation around Y and Z (see Figure 9): the greatest absolute displacement appears during the latter runs, with the third run being the most common one across all sub-populations. Unfortunately, no concrete explanation can be given for why this is the case. A reasonable hypothesis is that children get bored and exhausted as the image acquisition procedure advances, causing decreased focus and higher impulsivity.

In contrast to the spatial analysis of motion, there is little to no difference in behavior over time for the different sub-populations. The only cases where the two sexes showed a different run of greatest absolute displacement are for the 10-year-old's translation along Z (see Figure 8b) and rotation around X ((see Figure 9a and 9b) for both age groups. Moreover, the sub-populations often agree on the second most significant run and have a similar percentile split. These observations show that regardless of age and sex, children tend to move more toward the end of the scan and that their behavior over time can be predicted with a certain degree of confidence.

5.4 Correlation analysis

The correlation analysis (see Figure 10) aims to discover any underlying correlations between different DOFs and examine their relationships. Achieving that would complete the motion study, providing the clinic with another layer of motion pattern understanding. The analysis found several statistically significant correlations, but the discussion will revolve around the two pairs with the most significant positive/negative Pearson coefficient.

The most substantial positive correlation pair is translation along Y and rotation around X . Such motion would correspond to the subject moving their head up or down as they nod, a combination of movements that would make sense from a real-life standpoint. On the other hand, the strongest negative pair is translation along Y and translation along Z . From a scanner perspective, this would be the equivalent of the subject's head sinking into the pillow as they drift out of the bore. A noteworthy detail is that both pairs include one of the three DOFs that proved to be a dominant source of motion, further establishing the necessity of mitigating their effect.

Both pairs are visualized as 2D histograms in Figure 11a (translation along Y and rotation around X) and 11b (translation along Y and translation along Z). Both 2D distributions have a peak close to the origin and have a certain amount of symmetry. It is rather difficult to establish whether the symmetry is around the origin or whether it is around one of the axes. Such observation

is not surprising since the Pearson correlation of both 2D distributions is far from -1/+1 despite being the lowest/highest, respectively.

5.5 Limitations and future work

This paper has its limitations, primarily the dissimilarity between the size of the rsfMRI and DTI datasets. Such discrepancy can hinder the analysis and influence the significance of the observations in §3. Luckily, this issue will be resolved with the start of the thesis project itself; as of today’s data, the supervisor has downloaded everything available on the NDA.

Furthermore, despite the detailed image protocol provided by the ABCD study, it is impossible to consider every detail that might have occurred before or during scanning, inevitably interfering with the statistics.

Another limitation affects the temporal analysis, which, in this draft, considers only children with a particular number of runs. A better approach would be to calculate the exact duration of a scan by utilizing the number of frames (given by Figure 1a and 1b) and the duration a single one of them takes to be captured. This improvement is planned for the upcoming thesis project.

5.6 Code availability

The code is available on GitHub at the following link: <https://github.com/melanieganz/MoCoProject/tree/ABCDdev/ChildrenHeadMotionABCD>.

6 Conclusion

Given the discussed results and limitations, this project successfully builds on previously conducted research [1] [11] in its pursuit of understanding children’s head motion inside the MRI scanner. First and foremost, it establishes some statistically significant differences between the sexes’ motion traits, concluding that females are more cooperative than males. Furthermore, the project quantifies the behavior of children aged 9 and 10, establishing that the latter age group demonstrates increased self-control across the board. The temporal analysis in §5.3 is a novelty to the best of the author’s knowledge, and it confirms with a certain degree of confidence the rather intuitive conclusion that children move more during the later stages of image acquisition. Finally, the correlation analysis in §5.4 gave a different perspective on motion by finding intriguing underlying correlations between the DOFs.

The prevalent presence of translation along the Y and Z axes and rotation around the X axis should be diligently considered. A noteworthy observation is that the sources of motion mentioned above are substantially mitigated by introducing external stimuli in DTI imaging. Such an approach can replace general anesthesia for tasks that do not restrict children from keeping their eyes closed, which could benefit both the clinic via decreased manipulation costs and, most importantly, the patient by diminishing potential health complications that the repetitive implementation of anesthesia could introduce.

References

- [1] H. Eichhorn, A.-V. Vascan, M. Nørgaard, A. H. Ellegaard, J. M. Slipsager, S. H. Keller, L. Marner, and M. Ganz, “Characterisation of children’s head motion for magnetic resonance imaging with and without general anaesthesia,” *Frontiers in Radiology*, vol. 1, p. 789632, 2021.
- [2] M. Zaitsev, J. Maclarens, and M. Herbst, “Motion artifacts in mri: A complex problem with many partial solutions,” *Journal of Magnetic Resonance Imaging*, vol. 42, no. 4, pp. 887–901, 2015.
- [3] H. M. De Bie, M. Boersma, M. P. Wattjes, S. Adriaanse, R. J. Vermeulen, K. J. Oostrom, J. Huisman, D. J. Veltman, and H. A. Delemarre-Van de Waal, “Preparing children with a mock scanner training protocol results in high quality structural and functional mri scans,” *European journal of pediatrics*, vol. 169, pp. 1079–1085, 2010.
- [4] M. Jenkinson, P. Bannister, M. Brady, and S. Smith, “Improved optimization for the robust and accurate linear registration and motion correction of brain images,” *Neuroimage*, vol. 17, no. 2, pp. 825–841, 2002.
- [5] A. Davidson, “The effect of anaesthesia on the infant brain,” *Early human development*, vol. 102, pp. 37–40, 2016.
- [6] C. B. Paschal and H. D. Morris, “K-space in the clinic,” *Journal of Magnetic Resonance Imaging: An Official Journal of the International Society for Magnetic Resonance in Medicine*, vol. 19, no. 2, pp. 145–159, 2004.
- [7] R. Mezrich, “A perspective on k-space.,” *Radiology*, vol. 195, no. 2, pp. 297–315, 1995.
- [8] J. D. Power, K. A. Barnes, A. Z. Snyder, B. L. Schlaggar, and S. E. Petersen, “Spurious but systematic correlations in functional connectivity mri networks arise from subject motion,” *Neuroimage*, vol. 59, no. 3, pp. 2142–2154, 2012.
- [9] G. G. Slabaugh, “Computing euler angles from a rotation matrix,” *Retrieved on August*, vol. 6, no. 2000, pp. 39–63, 1999.
- [10] W. Yuan, M. Altaye, J. Ret, V. Schmithorst, A. W. Byars, E. Plante, and S. K. Holland, “Quantification of head motion in children during various fmri language tasks,” *Human brain mapping*, vol. 30, no. 5, pp. 1481–1489, 2009.
- [11] O. Afacan, B. Erem, D. P. Roby, N. Roth, A. Roth, S. P. Prabhu, and S. K. Warfield, “Evaluation of motion and its effect on brain magnetic resonance image quality in children,” *Pediatric radiology*, vol. 46, pp. 1728–1735, 2016.
- [12] R. K. Lenroot, N. Gogtay, D. K. Greenstein, E. M. Wells, G. L. Wallace, L. S. Clasen, J. D. Blumenthal, J. Lerch, A. P. Zijdenbos, A. C. Evans, *et al.*, “Sexual dimorphism of brain developmental trajectories during childhood and adolescence,” *Neuroimage*, vol. 36, no. 4, pp. 1065–1073, 2007.
- [13] C. L. Chapple and K. A. Johnson, “Gender differences in impulsivity,” *Youth violence and juvenile justice*, vol. 5, no. 3, pp. 221–234, 2007.
- [14] T. M. Olino, C. E. Durbin, D. N. Klein, E. P. Hayden, and M. W. Dyson, “Gender differences in young children’s temperament traits: Comparisons across observational and parent-report methods,” *Journal of personality*, vol. 81, no. 2, pp. 119–129, 2013.

Appendix

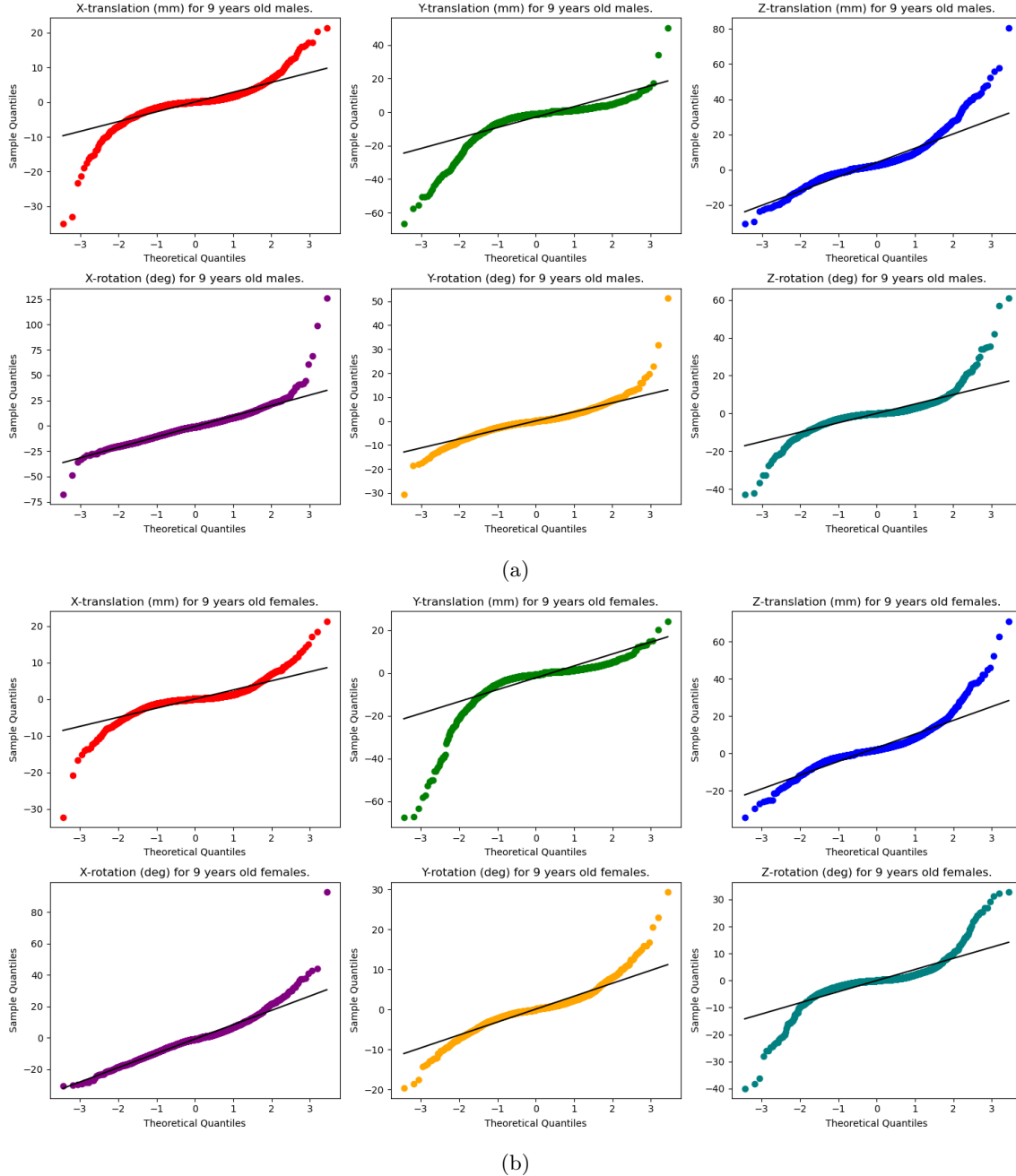
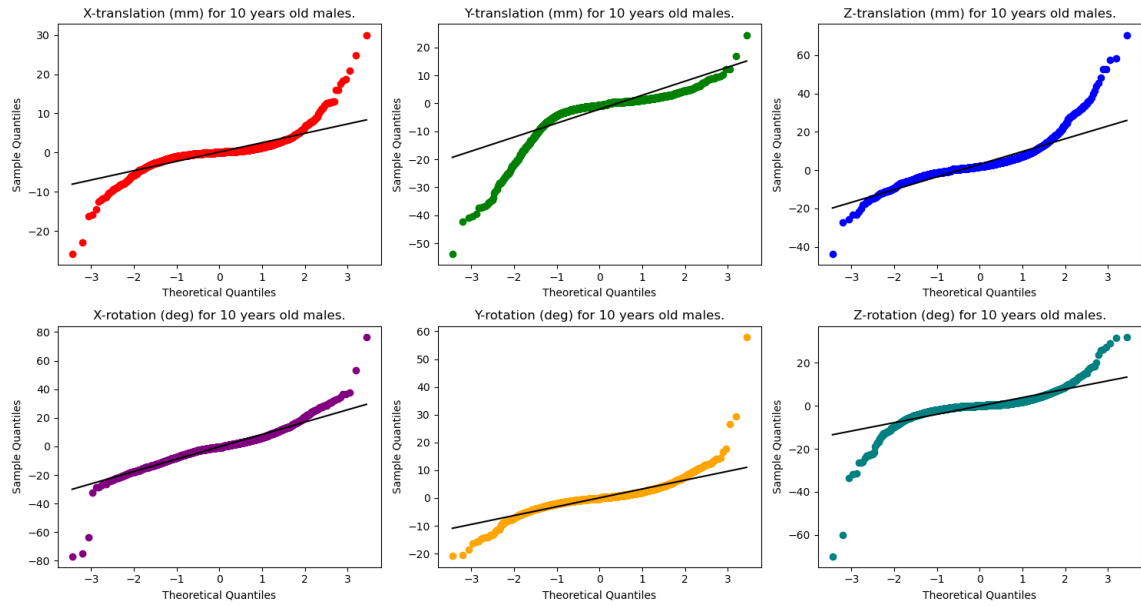
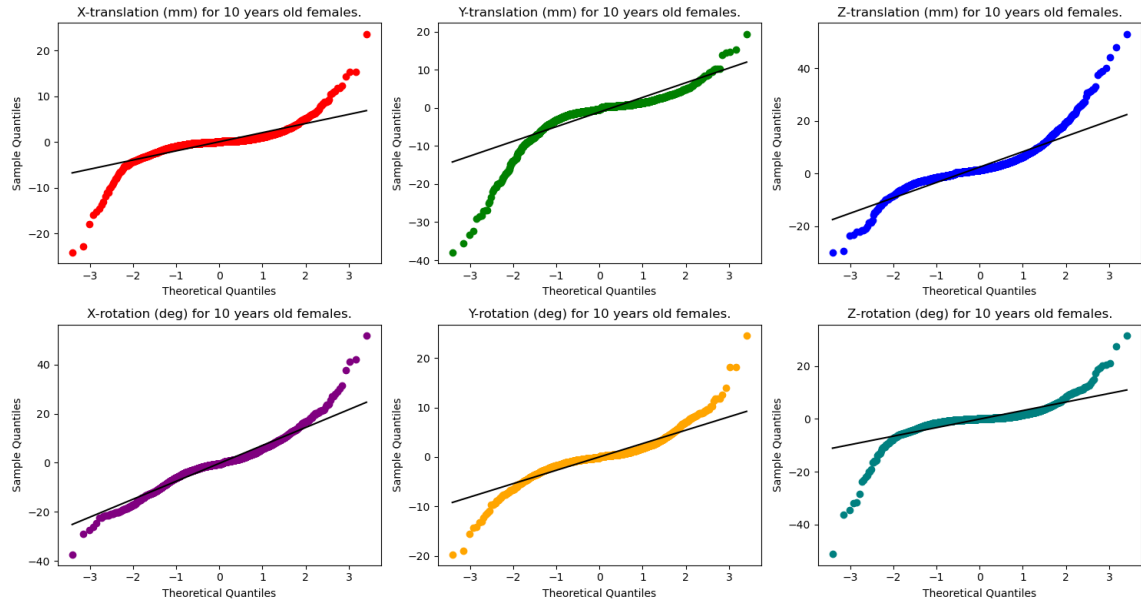


Figure 12: Q-Q plots of 9-year-old males (a) and females (b) rsfMRI distributions.

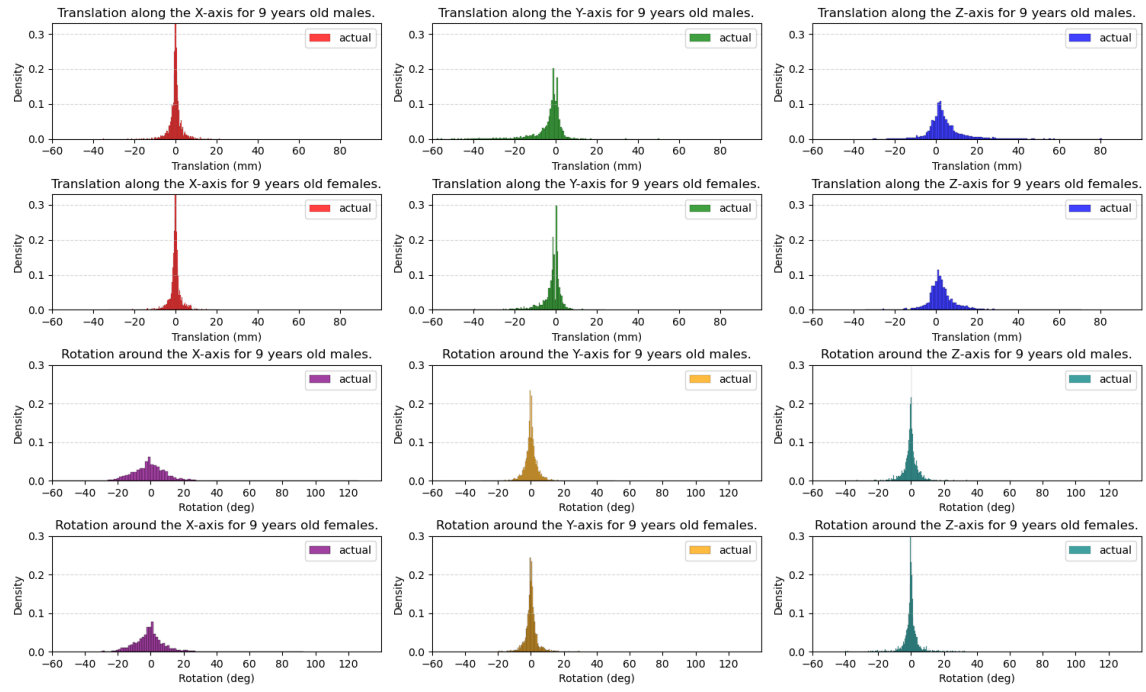


(a)

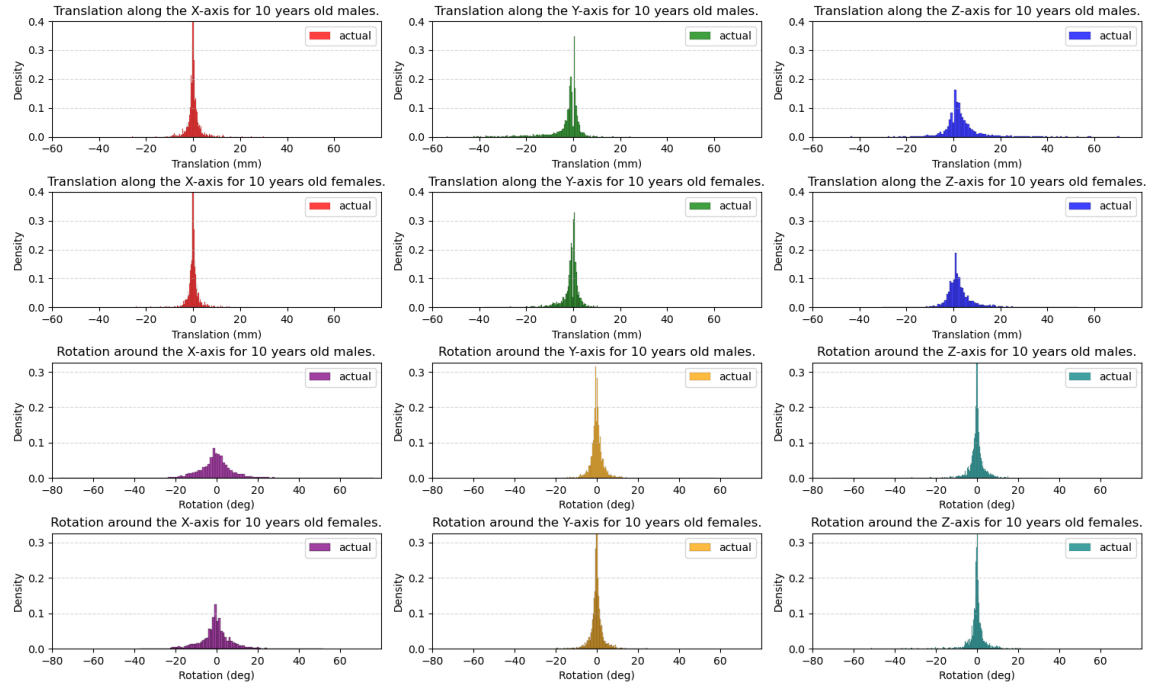


(b)

Figure 13: Q-Q plots of 10-year-old males (a) and females (b) rsfMRI distributions.



(a)



(b)

Figure 14: Distributions (rsfMRI) of 9-year-old males and females (a) and 10-year-old males and females (b).